# Utilizing an Improved Structure Analysis Method to Reveal Site-Specific Bonding Properties of Ag<sub>44</sub>(SR)<sub>30</sub> Nanoclusters

Ziyi Chen<sup>†</sup>, Daniel M. Chevrier<sup>†,1</sup>, Brian E. Conn<sup>‡,2</sup>, Terry P. Bigioni<sup>‡</sup>, Peng Zhang<sup>\*,†</sup>

<sup>1</sup> Current address is Aix-Marseille University, French Alternative Energies and Atomic Energy Commission (CEA), French National Center for Scientific Research (CNRS), UMR7265

Institute of Biosciences and Biotechnologies of Aix-Marseille (BIAM), Saint-Paul-lez-Durance, 13108 France

<sup>2</sup> Current address is

# **KEYWORDS**

silver nanoclusters, Ag<sub>44</sub>(SR)<sub>30</sub>, extended X-ray absorption fine structure (EXAFS), bonding properties, fitting method

<sup>&</sup>lt;sup>†</sup> Department of Chemistry, Dalhousie University, Halifax, Nova Scotia, B3H 4R2, Canada

<sup>&</sup>lt;sup>‡</sup> Department of Chemistry and Biochemistry, University of Toledo, Toledo, Ohio 43606, United States

### **ABSTRACT**

Atomically precise nanoclusters (NCs) are of great interest due to their molecule-like behaviour and unique physical and chemical properties. Understanding their structure-property relationship is an important task because it can help tailor their structures to achieve specific desired properties. In this study, the temperature-dependent bonding properties of Ag<sub>44</sub>(SR)<sub>30</sub> have been revealed by the extended X-ray absorption fine structure (EXAFS) with a new structure analysis method. It has been proved that the EXAFS fitting quality can be improved significantly compared with the conventional method. New insights into Ag-S bonding were discovered based on the fitting results obtained from the new method. Additionally, the metal core of Ag<sub>44</sub>(SR)<sub>30</sub> exhibits uncommon thermal behavior, which could be connected to the absence of a center atom in the icosahedral core. Our results demonstrate that the new structure analysis method can provide a more reliable comparison of NC structural changes than the conventional method and it could be applicable to other NCs. The revealed temperature-dependent bonding properties can provide insights into the structure-property relationship, which can help design new NCs materials with tailored properties.

### 1. INTRODUCTION

Atomically precise nanoclusters (NCs) have been studied for many years due to their unique physical and chemical properties.<sup>1-4</sup> Such NCs normally have size less than 2 nm and have a molecular structure, i.e. an exact number and arrangement of atoms in each NC. In recent years, more and more thiolate protected NCs has been synthesized and their structures were determined by single crystal X-ray diffraction.<sup>5-9</sup> Many of them possess structures that are not commonly observed in traditional nanoparticles.<sup>10-12</sup> Understanding their properties therefore becomes critical for developing a better understanding of the structure-property relationships and thereby determine their potential applications. Among the great variety of thiolate protected NCs, Ag NCs and Au NCs are two major groups in this field. However, the study of Ag NCs is less well-developed than Au NCs because of the lower stability of Ag NCs. In 2013, Na<sub>4</sub>Ag<sub>44</sub>(*p*-mercaptobenzoic acid)<sub>30</sub> (Ag<sub>44</sub>(SR)<sub>30</sub> for short) was shown to have such high stability that it could be synthesized in quantitative yields and on a large scale.<sup>6</sup> The study of structure and bonding properties under different conditions would be interesting since it could provide a deeper understanding of the stability of such materials.

X-ray absorption spectroscopy (XAS) is a powerful technique to study both electronic properties and bonding properties with only one spectrum.<sup>13</sup> The near edge region of XAS (XANES) has been successfully applied to investigate the electronic properties of NCs.<sup>14–17</sup> The extended X-ray absorption fine structure (EXAFS) is the region of XAS about 50 eV above the edge, which is useful for investigating the bonding properties of thiolate protected NCs under different conditions.<sup>18–22</sup> It has already been applied to study temperature effects on 25-atom NCs.<sup>20,21</sup> Generally, a thiolate protected NC could have several different coordination environments, and the bond distances can be grouped into various shells. The greatest advantage of EXAFS is that it

allows the observation of bond distance changes for each shell. Thus, the determination of fitting shells is a critical step. Simulated wavelet transformed EXAFS (WT-EXAFS) has been successfully applied to determine the fitting shells of EXAFS for Ag<sub>25</sub> NCs.<sup>21</sup> The WT-EXAFS have both information from FT-EXAFS and k space. When two types of bonds have similar bond distances, they can merge into one peak in FT-EXAFS, which can be resolved based on the wavenumber of k space in WT-EXAFS.<sup>23–25</sup> Most of the previous EXAFS studies on thiolate protected NCs focused on distinguishing the metal-metal (M-M) shells.<sup>19,20,22,26,27</sup> In this study, we present a Ag K-edge EXAFS analysis on solid phase Ag<sub>44</sub>(SR)<sub>30</sub> at 90 K and 300 K by using a new structure analysis method where two Ag-ligand shells were applied. The simulated WT-EXAFS method was utilized to determine the fitting shells. Then, the detailed structural changes on ligand-shell and M-M shell were uncovered from the fitting results of the new method.

# 2. METHODOLOGY

# 2.1 Synthesis of NCs

The detailed synthesis procedure of  $Ag_{44}(SR)_{30}$  NCs has been published previously.<sup>6</sup> Briefly, the Ag-thiolate precursor was synthesized by combining aqueous AgNO<sub>3</sub> with ethanolic *p*-mercaptobenzoic acid (*p*-MBA). Aqueous NaBH<sub>4</sub> was used to reduce the precursor to form the of  $Ag_{44}(SR)_{30}$  NCs. The NCs were isolated by precipitation with dimethylformamide (DMF).

# 2.2 XAS Measurements and Fitting Method

The Ag K-edge XAS spectra were collected at the Sector 20-BM beamline at the Advanced Photon Source (operating at 7.0 GeV). For data collected at 90 K, a helium-cooled cryostat chamber was used for measurements. The detailed description of the sample preparation for XAS measurements has been reported previously. The fitting of EXAFS spectra were performed by

Artemis and Athena.<sup>28</sup> The amplitude reduction factor  $(S_0^2)$  was fixed at 0.90, which was determined from a Ag foil reference. The  $k_2$ -weighting was applied for all fittings. For both the three-shell and four-shell fitting methods, a k-range of 3-12 Å<sup>-1</sup> was used. A fitting window of 1.5-3.5 Å was used for the three-shell and four-shell fitting methods for data collected at 90 K. A fitting window of 1-3 Å was applied for the four-shell fitting of data collected at 300 K. To reduce the number of variables, all coordination numbers (CNs) were fixed based on the crystal structure of  $Ag_{44}(SR)_{30}$ . The energy shift of all fitting shells was correlated for each fit. For the four-shell fitting method, the Debye-Waller factors of two Ag-S shells were correlated to further reduce the number of variables.

### 2.3 EXAFS Simulation and Wavelet Transformed EXAFS

The simulation of both Ag K-edge and S K-edge EXAFS spectra at 90 K was performed using the FEFF8 program code. <sup>29</sup> For the Ag K-edge simulation, different crystal structure models were used based on the separation of Ag-S shells. The simulation of S K-edge EXAFS included 44 Ag atoms and 30 S atoms as the structure model. The mount S and tail S atoms were selected as target atoms respectively. [[consider changing this sentence to: The S atoms in the bridging (1 atom) and base (4 atoms) positions in the capping mount motifs are chemically distinct and were selected as target atoms.]] The WT-EXAFS were generated by using a Morlet wave transform. <sup>30</sup> The k-range of 1-12.3 Å<sup>-1</sup> and 3-12 Å<sup>-1</sup> were used for the S K-edge and Ag K-edge, respectively. The wavelet parameters for S K-edge were set as 2.5 for  $\eta$  and 1 for  $\sigma$ , and  $\eta$ =4 and  $\sigma$ =1 were used for the Ag K-edge in order to have high resolution in k space.

# 3. RESULTS AND DISCUSSION

# **Determination of fitting shells**

The FT-EXAFS spectra of Ag K-edge for Ag<sub>44</sub>(SR)<sub>30</sub> at two different temperatures are shown in Figure 1. The peak at around 2 Å is attributed to the Ag-S bonds. The peak appearing at around 2.7 Å corresponds to the Ag-Ag bonds. The peak intensity of FT-EXAFS spectrum is mainly affected by the size of NCs and the Debye-Waller factor. In this study, the difference in peak intensity at the two different temperatures comes from the Debye-Waller factor. At the lower temperature, thermal fluctuations are suppressed, which can lead to a smaller Debye-Waller factor and therefore higher peak intensities in the FT-EXAFS spectrum.<sup>31</sup>

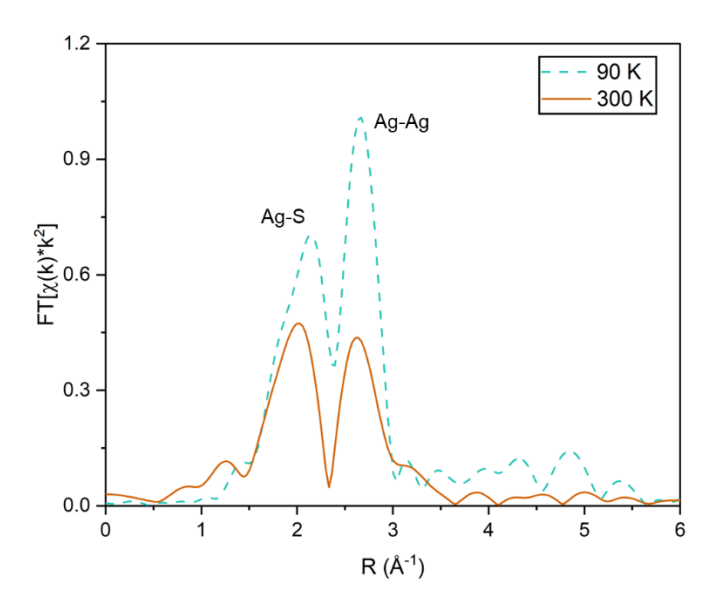
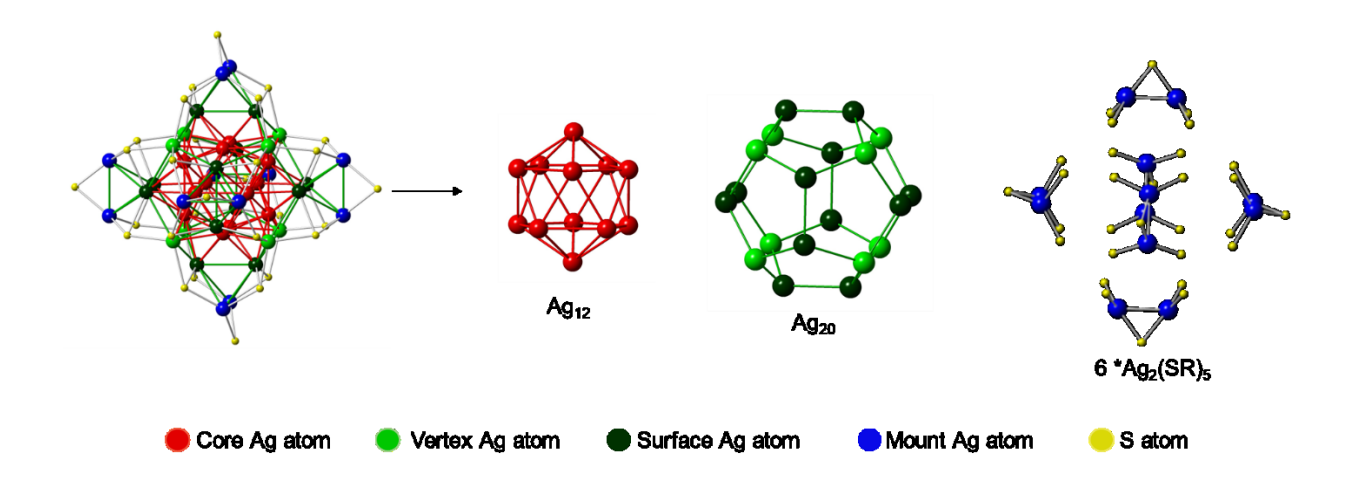


**Figure 1.** Ag K-edge FT-EXAFS spectra of  $Ag_{44}(SR)_{30}$  at 90 K and 300 K. [[the x-axis units are Å<sup>-1</sup> but should be Å]]

In order to get detailed structural information from fitting the FT-EXAFS spectra of Ag<sub>44</sub>(SR)<sub>30</sub>, the site-specific bonding in the molecule was first analyzed<sup>18,20,26</sup> using the structure that was experimentally measured by single-crystal x-ray diffraction.<sup>6</sup> [[I assume the data in figures 2 and 3 are taken from the experimental crystal structure? Is that right? Temp was 150 K.]] As shown in Scheme 1, the structure can be broken down into a hollow icosahedral Ag<sub>12</sub> inner metal core, a

dodecahedral Ag<sub>20</sub> cage, and six Ag<sub>2</sub>(SR)<sub>5</sub> mount motifs. It should be noticed that the 20 Ag atoms in the cage can be further distinguished into two chemically different sites due to the placement of the 6 capping mount motifs. Within the Ag<sub>20</sub> structure, there are eight Ag atoms (light green atoms in Scheme 1) that can be considered as vertices of a cube, which are each bonded to 3 S atoms. The remaining 12 Ag atoms in the Ag<sub>20</sub> structure can be grouped into six pairs, which are located above each face of the cube and are bonded to 2 S atoms. Thus, there are four different Ag coordination environments.



**Scheme 1.** The crystal structure of Ag<sub>44</sub>(SR)<sub>30</sub> NCs with the indication of different Ag sites. The hydrocarbon portions of the thiolate ligands were omitted for clarity. [[You could consider making the base S and bridging S different colours, with corresponding "Base S atom" and "Bridging S atom" labels, since they are in chemically different environments]]

From inspection of the Ag-Ag bond length distribution (Figure 2), two distinct shells were identified. The first Ag-Ag shell (Ag-Ag1) consists of strong metallic bonds within the Ag<sub>12</sub> core as well as bonds that link the Ag<sub>12</sub> metal core to the Ag<sub>20</sub> cage, which are consistent with the bulk Ag-Ag bond length. The second Ag-Ag shell (Ag-Ag2) are longer bonds that connect vertex, surface and mount Ag sites.

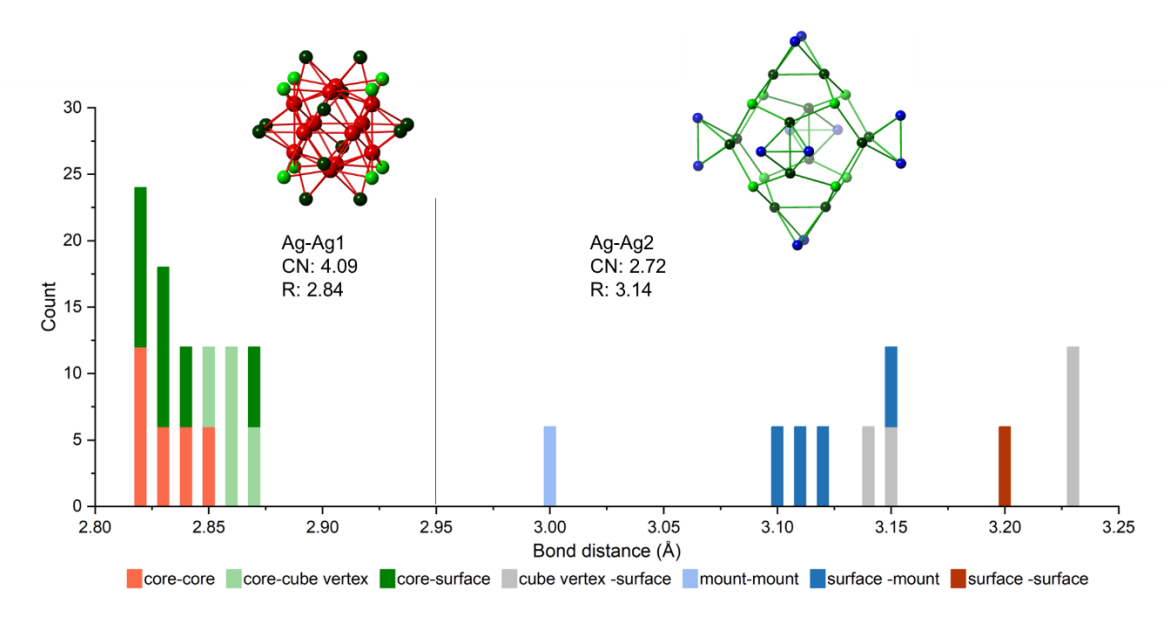


**Figure 2.** The bond length distribution of Ag-Ag bonds of Ag44(SR)<sub>30</sub> with assigned FT-EXAFS fitting shells. The Ag-Ag1 bonds are those that connect the 12 Ag atoms in the icosahedral inner shell to one another as well as those that connect each Ag atom to the 20 faces of the icosahedron. The Ag-Ag2 bonds are those that connect the 20 Ag atoms in the decahedral outer shell to one another as well as those that connect six pairs of Ag atoms that straddle pairs of Ag atoms in the decahedron. [[what temperature?]] [[it would be cool if the different bonds were the same color as the corresponding bar in the bar graph – would help \*see\* – if that is possible]] [[bigger structures would be helpful to the reader]] [[are these distances from crystal structure data? Or based on simulations/DFT?]]

Since the Ag<sub>44</sub>(SR)<sub>30</sub> NCs have 3D mount motifs, the S atoms could also experience different coordination environments, therefore it is worthwhile examining the Ag-S bond length distribution. As displayed in Figure 3, there are two Ag-S shells. The 1<sup>st</sup> shell includes the bonds between the S atoms in the base of the mounts to the mount Ag and the surface Ag atoms. The 2<sup>nd</sup> shell includes the bonds between the S atoms in the base of the mounts to the vertex Ag atoms. The S atoms bonded to two mount Ag atoms (bridging S) are different from the remaining S atoms (base S).

[[I now see that I might be creating a terminology issue with the S atoms, so feel free to reject my terminology/change back to your terminology – sorry if I created a problem for you]]

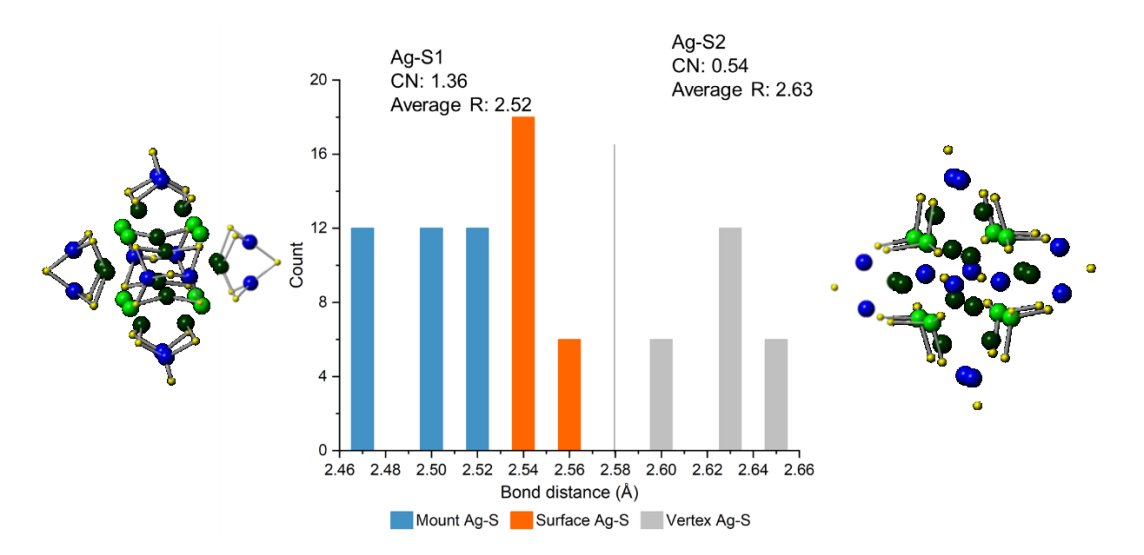


**Figure 3.** The bond length distribution of Ag-S bonds of Ag<sub>44</sub>(SR)<sub>30</sub> with assigned FT-EXAFS fitting shells. (Yellow: S atom; blue: mount Ag atoms; dark green: surface Ag atoms; light green: vertex Ag atoms) [[what temperature?]] [[it would be cool if the different bonds were the same color as the corresponding bar in the bar graph (to help \*see\* correspondence), if possible]] [[what about bond distances between the mount Ag atoms and the bridging S atoms (not shown)? They tend to be slightly shorter than the distances between the mount Ag atoms and the base S atoms (here labeled "Mount Ag-S"), but in the same 2.45-2.5 A range, so would overlap in this figure.]] [[bigger structures would be helpful to the reader]]

To verify if the two Ag-S shells are distinguishable in EXAFS, both S K-edge and Ag K-edge WT-EXAFS simulations were performed. For the S K-edge WT-EXAFS simulations, the major signal areas were found to have different shapes for the two different S sites (Figure 4). For the bridging S, there is only one area at around k ~4 Å<sup>-1</sup>. This suggests that there is only one type of Ag-S bond between the bridging S atoms and the mount Ag atoms, which is consistent with all mount Ag atoms being in chemically equivalent positions. For the base S atoms, however, the major signal area is at the same position but it splits into two partially joined areas. This indicates that there are two types of bonds despite the fact that each base S atom is bonded to three chemically inequivalent Ag atoms: mount Ag, surface Ag, and vertex Ag. Although one may expect to observe three distinct types of bonds, the mount Ag-S and surface Ag-S bond lengths are close enough to merge into one Ag-S shell. The vertex Ag-S bonds are significantly longer,

however, such that they represent a distinct Ag-S shell. Hence, only two distinct areas are observed for the base S atom bonding. [[note to self: what does this mean for distinguishing base from bridge if both are centered at  $k \sim 4 \text{ Å}^{-1}$ ? Are they distinguishable using the S K-edge based on the splitting? Or is the overlap too great?]]

WT-EXAFS simulations were also performed for the two Ag-S shells using the Ag K-edge, to investigate if they are separatable from an Ag perspective. As shown in Figure 5, the center of the strongest signal from the two shells appears at different k values, indicating that the two Ag-S shells should be distinguishable in EXAFS using the Ag K-edge.

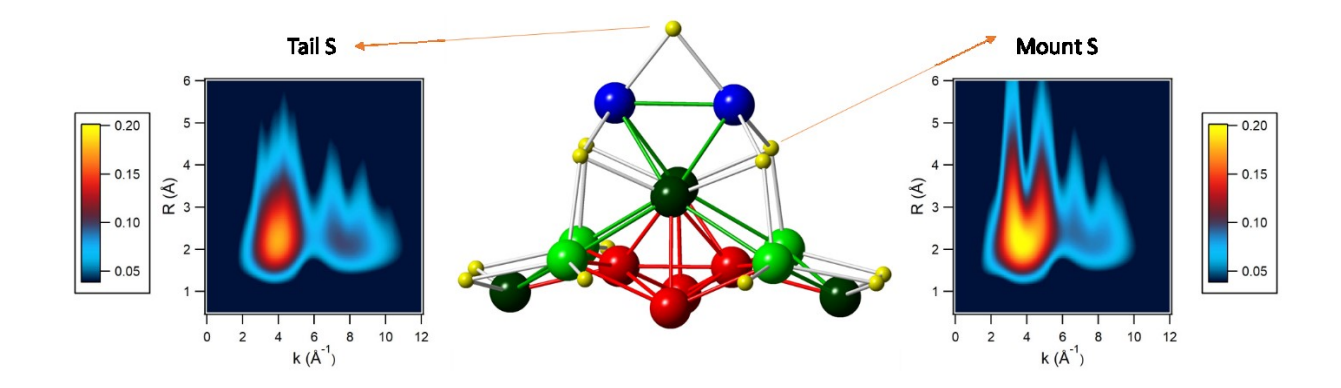


**Figure 4.** The WT-EXAFS simulations of S K-edge for the two distinct S sites.

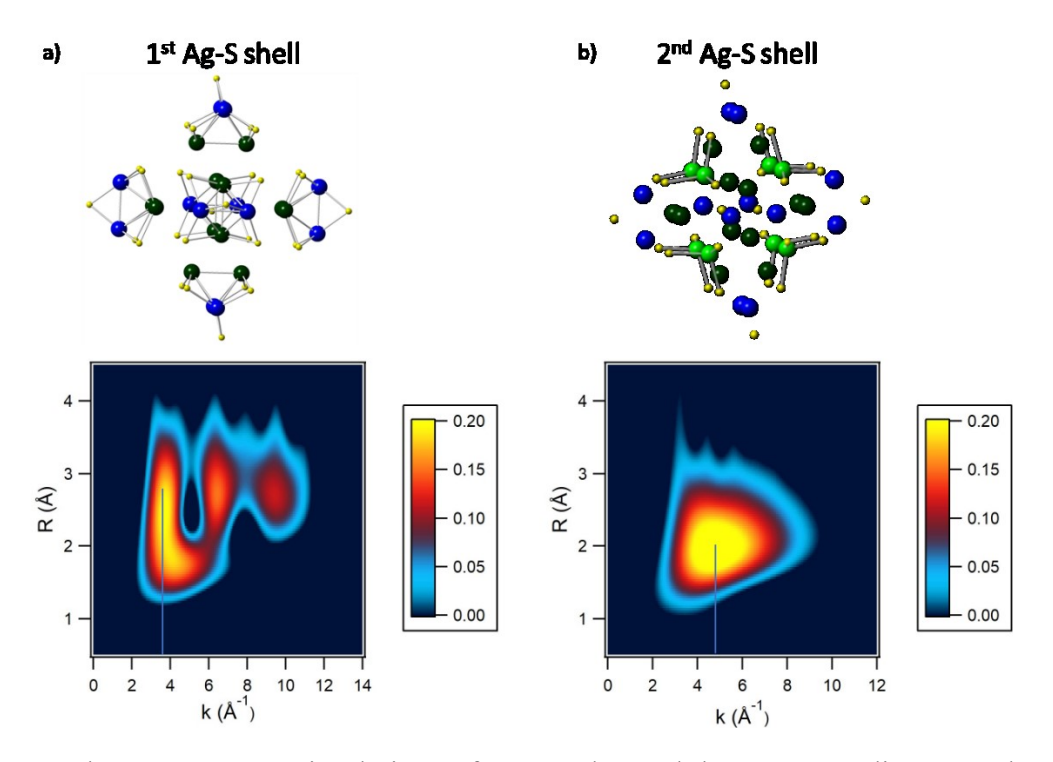


**Figure 5.** The WT-EXAFS simulations of Ag K-edge and the corresponding crystal structure for a) the Ag-S1 shell and b) the Ag-S2 shell. [[these are referred to elsewhere as Ag-S1 and Ag-S2, so it may be better to use that same nomenclature here]]

# Fitting method comparison

Based on the analysis of fitting shells, two Ag-S shells and two Ag-Ag shells were identified. The four-shell fitting method was therefore applied to the data collected at 90 K and 300 K and the fitting results were compared with the traditional three-shell fitting method (one Ag-S shell and two Ag-Ag shells). Figure 6a and b show the fits by using four shells, which are similar to the fits obtained by using three shells (Figure S1). However, these two methods show obvious differences in Debye-Waller factors and R-factors, which are two parameters related to the fitting quality of EXAFS. The Debye-Waller factors can indicate the variation of bond length within a shell. If one shell contains bonds with a narrow range, the Debye-Waller factor will be small and it can be considered to be a good fit. From the comparison of four-shell and three-shell fitting methods, the Debye-Waller factors of the Ag-S shell and the Ag-Ag2 shell become smaller when

two Ag-S shells were used (see Fig. 6c). The R-factor is a statistical value to evaluate the differences between the fitting curve and experimental data. Typically, a good fit should have an R-factor that is less than 0.03. In this study, the R-factors can be reduced by applying the four-shell fitting method (Table 1). Particularly, the R-factor of 300 K data using the conventional three-shell method is 0.031, which is at the margin of an acceptable fitting result. By applying the new four-shell method, the R-factor was decreased to 0.013. The decreases of Debye-Waller factors and R-factors further indicate the necessity of using two Ag-S shells. Moreover, the decreases are more pronounced for data collected at 300 K, which means the noisy data are more sensitive to the fitting method. The Debye-Waller factor of the Ag-Ag1 shell is essentially the same for the results from the two methods, suggesting the shell with larger CN is tolerant of different fitting methods [[is higher CN the reason or is it because there are a large number of Ag-Ag1 bonds of the same length?]]. Thus, we can conclude that the determination of fitting shells is critical[[important?]] for noisy data and for the fitting of shells with small CNs.

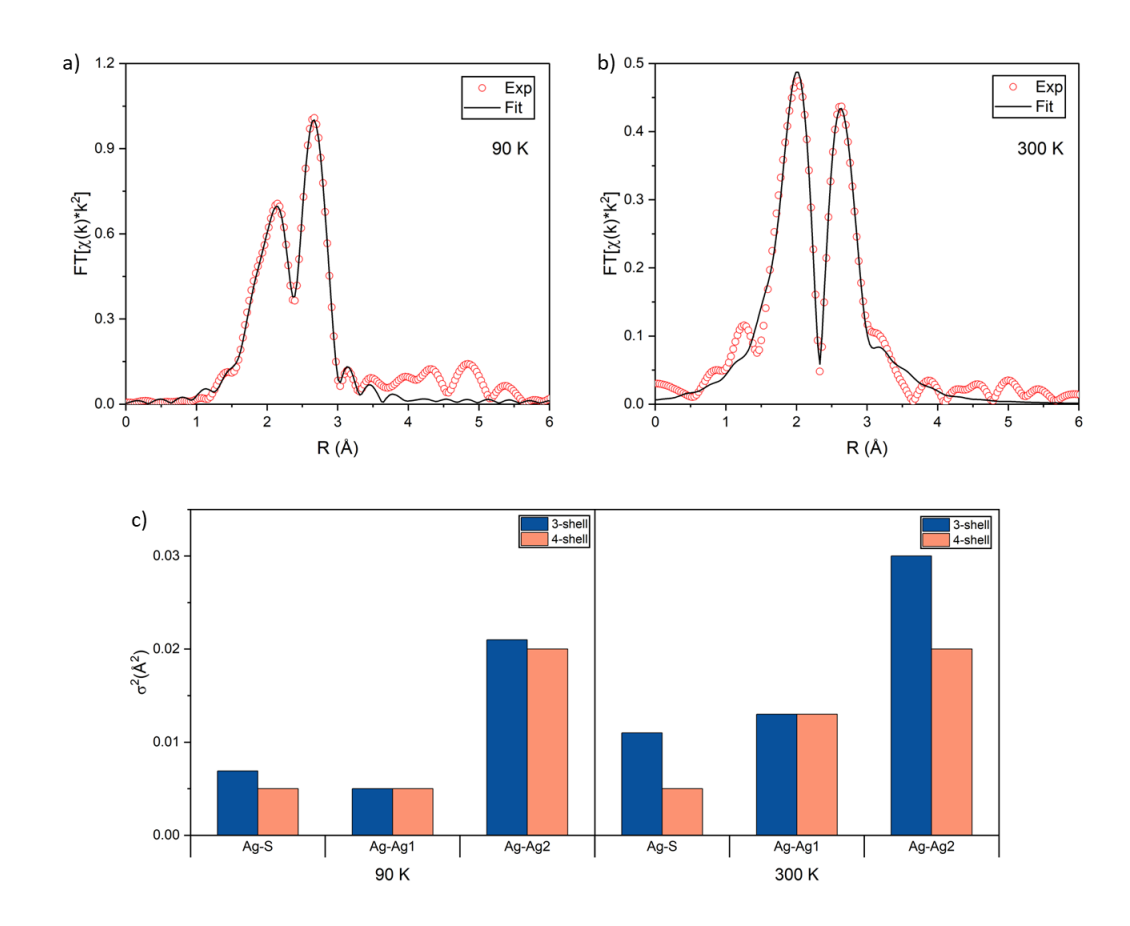


**Figure 6.** Ag K-edge FT-EXAFS spectrum of Ag<sub>44</sub>(SR)<sub>30</sub> with four-shell fitting at a) 90 K and b) 300K. c) The comparison of Debye-Wall factors obtained by two fitting methods. The Debye-Waller factors for two Ag-S shells were correlated for four-shell fitting method. (Left panel: 90 K; right panel: 300K) [[I'm confused: Ag-S has been used to represent one Ag/S shell in the three shell model but here the pair of bars on the left indicate Ag-S Debye-Waller factors for both one (blue) and two (orange) Ag/S shells. In this case, does the orange bar represent the average Debye-Waller factors for the Ag-S1 and Ag-S2 shells in the four shell model?]]

# Temperature effect on ligand shell and metal core

The EXAFS fitting results of bonding distances from the two methods are plotted in Figure 7a-c. Comparing the trend observed from three-shell and four-shell fitting methods, the Ag-S shells show different results (Figure 7a). When only one Ag-S shell was applied, the Ag-S bonds showed small contractions as the temperature increased from 90 K to 300 K. However, when two

Ag-S shells were included, the bond distances of the Ag-S1 shell were unchanged while the bond distances of the Ag-S2 shell increased when the temperature changed from 90 K to 300 K.

From the crystal structure, the Ag-S1 shell consists of Ag-S bonds within the mount motifs, which can be regulated by thiolate ligands. The unchanged bond distances indicate the existence of a rigid ligand shell in Ag<sub>44</sub>(SR)<sub>30</sub>, which might contribute to the stability of these NCs. The Ag-S2 shell represents the linkage between mount motifs and the Ag<sub>32</sub> core structure, which appear to be more flexible compared with the Ag-S1 bonds within mount motifs. The idea of separation of ligand shell from the Ag<sub>32</sub> metal core is similar to the concept of rigid rings in thiolate protected Au NCs.<sup>32–34</sup>

In addition, the distinct nature of each type of Ag-S bonds can result in different thermal behavior. The metallic nature of the Ag sites decreases when moving outward, away from the Ag<sub>12</sub> metal core, which can affect Ag-S bonding. In particular, the vertex Ag atoms have more metallic characteristics than the surface and mount Ag atoms such that when they form bonds with S atoms, the Ag-S bonds can exhibit normal expansion behavior [[does TEC depend on metallicity of Ag in Ag-S bonds?]]. The increase of the Ag-S2 shell bond distances at a higher temperature cannot be observed in the one Ag-S shell fitting results because the contribution of the Ag-S2 shell to the overall Ag-S shell is small, due to its low CN of 0.54. Thus, it is important to separate the Ag-S shells into two shells for the analysis of EXAFS.

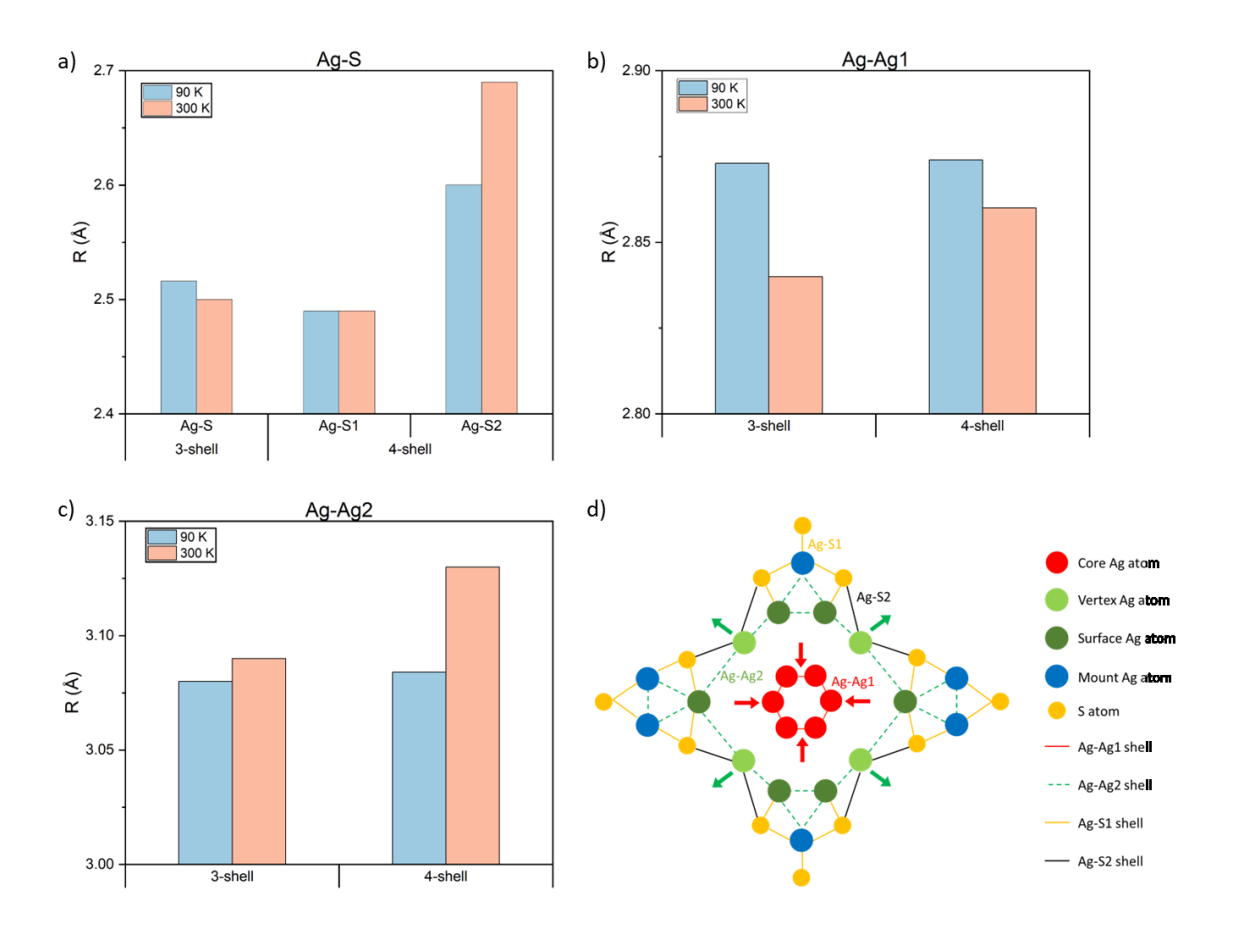


**Figure 7.** The comparison of bond distances at different temperatures by using 3-shell and 4-shell fitting methods for a) Ag-S shells, b) Ag-Ag1 shell and c) Ag-Ag2 shell. d) Schematic illustration of each shell with indicated bond distance changes upon temperature increase.

On the other hand, the Ag-Ag shells show similar trends between these two methods, although their magnitudes differ. The Ag-Ag1 shell shows bond contraction, and the Ag-Ag2 shell shows bond expansion as the temperature increases (Figure 7b-d). The negative thermal expansion exhibited by the metal core is not commonly observed in thiolate protected NCs. For Au<sub>25</sub>, its structure contains of an icosahedral Au<sub>13</sub> metal core, which experiences a bond expansion with the increase of temperature.<sup>20</sup> The unique behavior of Ag<sub>44</sub>(SR)<sub>30</sub> metal core could be due to the one atom absence at the center.

 $\textbf{Table 1}. \ EXAFS \ Three-shell \ (top) \ and \ Four-shell \ (bottom) \ Fitting \ Results \ for \ Ag_{44}(SR)_{30} \ NCs \ at \ 90 \ K \ and \ 300 \ K$ 

Temperature (K)	Shell	CN (fixed)	R (Å)	$\sigma^2$ (Å <sup>2</sup> )	ΔE <sub>0</sub> (eV)	R factor
90	Ag-S	1.9	2.516 (5)	0.0069 (6)	3.5 (4)	0.0015
	Ag-Ag1	4.09	2.873 (2)	0.0050(2)		
	Ag-Ag2	2.72	3.08 (2)	0.021 (4)		
300	Ag-S	1.9	2.50 (2)	0.011 (2)	2 (2)	0.031
	Ag-Ag1	4.09	2.84 (2)	0.013 (1)		
	Ag-Ag2	2.72	3.09 (6)	0.03 (1)		
90	Ag-S1	1.36	2.490 (8)	0.005 (2)	3.6 (5)	0.0013
	Ag-S2	0.54	2.60 (4)			
	Ag-Ag1	4.09	2.874 (3)	0.0050(2)		
	Ag-Ag2	2.72	3.084 (4)	0.020 (4)		
300	Ag-S1	1.36	2.49 (2)	0.005 (1)		
	Ag-S2	0.54	2.69 (4)		4 (2)	0.013
	Ag-Ag1	4.09	2.86 (2)	0.013 (1)		
	Ag-Ag2	2.72	3.13 (5)	0.02(1)		

# 4. CONCLUSIONS

In conclusion, the bonding properties of  $Ag_{44}(SR)_{30}$  have been examined via EXAFS from a site-specific perspective. The WT-EXAFS simulations were helpful for the determination of fitting shells. It was found that there are two Ag-S shells and two Ag-Ag shells in  $Ag_{44}(SR)_{30}$ . The four-

shell fitting method was applied to the data collected at 90 K and 300 K. This new structure analysis method shows significantly increased EXAFS fitting quality as evidenced by improved R-factor and Debye-Waller factors. Given the improvement of the fitting for Ag<sub>44</sub>(SR)<sub>30</sub> at both temperatures, the close comparison of bond distance change due to temperature effects is more reliable. It shows that the vertex Ag-S2 bonds exhibit a considerable increase of bond distance, which is different from surface and mount Ag-S1 bonds. The metal core of Ag<sub>44</sub>(SR)<sub>30</sub> shows negative thermal expansion, which is not common to NCs and could be attributed to the absence of a center atom in the icosahedral core. It also suggests a possible structure-function relationship that could guide the development of new NC materials, such as removing one atom or doping with different atoms. The new EXAFS fitting method developed in this work can be extended to the analysis of other NCs, which can provide more reliable structure details for comparison. The uncovered temperature-dependent bonding properties by new the method could provide insights into the structure-property relationship, which can also help with the design of new NC materials with desired properties.

# ASSOCIATED CONTENT

# **Supporting Information.**

The following files are available free of charge.

Supporting figures of Ag K-edge FT-EXAFS spectrum of Ag<sub>44</sub>(SR)<sub>30</sub> with three-shell fitting at 90 K and 300K. (PDF)

### AUTHOR INFORMATION

# **Corresponding Authors**

Peng Zhang – Department of Chemistry, Dalhousie University, Halifax, NS B3H 4R2, Canada; E-mail: peng.zhang@dal.ca

# **Authors**

Ziyi Chen – Department of Chemistry, Dalhousie University, Halifax, NS B3H 4R2, Canada

Daniel M. Chevrier – Aix-Marseille University, French Alternative Energies and Atomic Energy

Commission (CEA), French National Center for Scientific Research (CNRS), UMR7265

Institute of Biosciences and Biotechnologies of Aix-Marseille (BIAM), Saint-Paul-lez-Durance,

13108 France

Brian E. Conn –

Terry P. Bigioni – Department of Chemistry and Biochemistry, University of Toledo, Toledo, Ohio 43606, United States

# **Notes**

The authors declare no competing financial interests.

### **ACKNOWLEDGMENTS**

The authors would like to thank the financial support from NSERC Canada. This research used resources of the Advanced Photon Source, an Office of Science User Facility operated for the US Department of Energy (DOE) Office of Science by Argonne National Laboratory, and was supported by the US DOE under contract no. DE-AC02-06CH11357, and the Canadian Light Source (CLS) and its funding partners. The CLS is supported by the CFI, NSERC, NRC, CIHR, the University of Saskatchewan, the Government of Saskatchewan, and Western Economic Diversification Canada. Z.C. would like to acknowledge the PhD Entrance scholarship from Dalhousie University and the Nova Scotia Graduate Scholarship – Doctoral. T.P.B. thanks the National Science Foundation for financial support (Grant No. 1905262).

# REFERENCES

- (1) Du, Y.; Sheng, H.; Astruc, D.; Zhu, M. Atomically Precise Noble Metal Nanoclusters as Efficient Catalysts: A Bridge between Structure and Properties. *Chem. Rev.* **2020**, *120*, 526–622. DOI: 10.1021/acs.chemrev.8b00726.
- (2) Kang, X.; Li, Y.; Zhu, M.; Jin, R. Atomically Precise Alloy Nanoclusters: Syntheses, Structures, and Properties. *Chem. Soc. Rev.* **2020**, *49*, 6443–6514. DOI: 10.1039/C9CS00633H.
- (3) Walsh, A. G.; Zhang, P. Thiolate-Protected Bimetallic Nanoclusters: Understanding the Relationship between Electronic and Catalytic Properties. *J. Phys. Chem. Lett.* **2021**, *12*, 257–275. DOI: 10.1021/acs.jpclett.0c03252.
- (4) Walsh, A. G.; Zhang, P. Thiolate-Protected Single-Atom Alloy Nanoclusters: Correlation between Electronic Properties and Catalytic Activities. *Adv. Mater. Interfaces* **2021**, *8*, 2001342. DOI: 10.1002/admi.202001342.
- (5) Joshi, C. P.; Bootharaju, M. S.; Alhilaly, M. J.; Bakr, O. M. [Ag<sub>25</sub>(SR)<sub>18</sub>]<sup>-</sup>: The "Golden" Silver Nanoparticle. *J. Am. Chem. Soc.* **2015**, *137*, 11578–11581. DOI: 10.1021/jacs.5b07088.
- (6) Desireddy, A.; Conn, B. E.; Guo, J.; Yoon, B.; Barnett, R. N.; Monahan, B. M.; Kirschbaum, K.; Griffith, W. P.; Whetten, R. L.; Landman, U.; Bigioni, T. P. Ultrastable Silver Nanoparticles. *Nature* **2013**, *501*, 399–402. DOI: 10.1038/nature12523.
- (7) Qian, H.; Eckenhoff, W. T.; Zhu, Y.; Pintauer, T.; Jin, R. Total Structure Determination of Thiolate-Protected Au<sub>38</sub> Nanoparticles. *J. Am. Chem. Soc.* **2010**, *132*, 8280–8281. DOI: 10.1021/ja103592z.
- (8) Yang, H.; Wang, Y.; Huang, H.; Gell, L.; Lehtovaara, L.; Malola, S.; Häkkinen, H.; Zheng, N. All-Thiol-Stabilized Ag<sub>44</sub> and Au<sub>12</sub>Ag<sub>32</sub> Nanoparticles with Single-Crystal Structures. *Nat. Commun.* **2013**, *4*, 2422. DOI: 10.1038/ncomms3422.
- (9) Wan, X.-K.; Wang, J.-Q.; Wang, Q.-M. Ligand-Protected Au<sub>55</sub> with a Novel Structure and Remarkable CO<sub>2</sub> Electroreduction Performance. *Angew. Chem. Int. Ed.* **2021**, *60*, 20748–20753. DOI: 10.1002/anie.202108207.
- (10) Higaki, T.; Li, Y.; Zhao, S.; Li, Q.; Li, S.; Du, X.-S.; Yang, S.; Chai, J.; Jin, R. Atomically Tailored Gold Nanoclusters for Catalytic Application. *Angew. Chem.* **2019**, *131*, 8377–8388. DOI: 10.1002/ange.201814156.
- (11) Xie, Y.-P.; Shen, Y.-L.; Duan, G.-X.; Han, J.; Zhang, L.-P.; Lu, X. Silver Nanoclusters: Synthesis, Structures and Photoluminescence. *Mater. Chem. Front.* **2020**, *4*, 2205–2222. DOI: 10.1039/D0QM00117A.
- (12) Cowan, M. J.; Mpourmpakis, G. Structure–Property Relationships on Thiolate-Protected Gold Nanoclusters. *Nanoscale Adv.* **2019**, *1*, 184–188. DOI: 10.1039/C8NA00246K.
- (13) Zhang, P. X-Ray Spectroscopy of Gold–Thiolate Nanoclusters. *J. Phys. Chem. C* **2014**, *118*, 25291–25299. DOI: 10.1021/jp507739u.
- (14) Chen, Z.; Walsh, A. G.; Wei, X.; Zhu, M.; Zhang, P. Site-Specific Electronic Properties of [Ag<sub>25</sub>(SR)<sub>18</sub>]<sup>-</sup> Nanoclusters by X-Ray Spectroscopy. *Small* **2021**, *17*, 2005162. DOI: 10.1002/smll.202005162.
- (15) Christensen, S. L.; MacDonald, M. A.; Chatt, A.; Zhang, P.; Qian, H.; Jin, R. Dopant Location, Local Structure, and Electronic Properties of Au<sub>24</sub>Pt(SR)<sub>18</sub> Nanoclusters. *J. Phys. Chem. C* **2012**, *116*, 26932–26937. DOI: 10.1021/jp310183x.

- (16) Chevrier, D. M.; Zeng, C.; Jin, R.; Chatt, A.; Zhang, P. Role of Au<sub>4</sub> Units on the Electronic and Bonding Properties of Au<sub>28</sub>(SR)<sub>20</sub> Nanoclusters from X-Ray Spectroscopy. J. Phys. Chem. C 2015, 119, 1217–1223. DOI: 10.1021/jp509296w.
- (17) Chevrier, D. M.; MacDonald, M. A.; Chatt, A.; Zhang, P.; Wu, Z.; Jin, R. Sensitivity of Structural and Electronic Properties of Gold–Thiolate Nanoclusters to the Atomic Composition: A Comparative X-Ray Study of Au<sub>19</sub>(SR)<sub>13</sub> and Au<sub>25</sub>(SR)<sub>18</sub>. *J. Phys. Chem. C* 2012, 116, 25137–25142. DOI: 10.1021/jp309283y.
- (18) Chevrier, D. M.; Conn, B. E.; Li, B.; Jiang, D.; Bigioni, T. P.; Chatt, A.; Zhang, P. Interactions between Ultrastable Na<sub>4</sub>Ag<sub>44</sub>(SR)<sub>30</sub> Nanoclusters and Coordinating Solvents: Uncovering the Atomic-Scale Mechanism. *ACS Nano* **2020**, *14*, 8433–8441. DOI: 10.1021/acsnano.0c02615.
- (19) MacDonald, M. A.; Zhang, P.; Chen, N.; Qian, H.; Jin, R. Solution-Phase Structure and Bonding of Au<sub>38</sub>(SR)<sub>24</sub> Nanoclusters from X-Ray Absorption Spectroscopy. *J. Phys. Chem. C* **2011**, *115*, 65–69. DOI: 10.1021/jp1102884.
- (20) MacDonald, M. A.; Chevrier, D. M.; Zhang, P.; Qian, H.; Jin, R. The Structure and Bonding of Au<sub>25</sub>(SR)<sub>18</sub> Nanoclusters from EXAFS: The Interplay of Metallic and Molecular Behavior. *J. Phys. Chem. C* **2011**, *115*, 15282–15287. DOI: 10.1021/jp204922m.
- (21) Chen, Z.; Walsh, A. G.; Wei, X.; Zhu, M.; Zhang, P. New Insights into the Bonding Properties of [Ag<sub>25</sub>(SR)<sub>18</sub>] Nanoclusters from X-Ray Absorption Spectroscopy. *J. Phys. Chem. C* **2022**, *126*, 12721–12727. DOI: 10.1021/acs.jpcc.2c04482.
- Yang, R.; Chevrier, D. M.; Zeng, C.; Jin, R.; Zhang, P. Bonding Properties of FCC-like Au<sub>44</sub>(SR)<sub>28</sub> Clusters from X-Ray Absorption Spectroscopy. *Can. J. Chem.* **2017**, *95*, 1220–1224. DOI: 10.1139/cjc-2017-0169.
- (23) Funke, H.; Chukalina, M.; Scheinost, A. C. A New FEFF-Based Wavelet for EXAFS Data Analysis. *J. Synchrotron Radiat.* **2007**, *14*, 426–432. DOI: 10.1107/S0909049507031901.
- (24) Penfold, T. J.; Tavernelli, I.; Milne, C. J.; Reinhard, M.; Nahhas, A. E.; Abela, R.; Rothlisberger, U.; Chergui, M. A Wavelet Analysis for the X-Ray Absorption Spectra of Molecules. *J. Chem. Phys.* **2013**, *138*, 014104. DOI: 10.1063/1.4772766.
- (25) Martini, A.; Signorile, M.; Negri, C.; Kvande, K.; Lomachenko, K. A.; Svelle, S.; Beato, P.; Berlier, G.; Borfecchia, E.; Bordiga, S. EXAFS Wavelet Transform Analysis of Cu-MOR Zeolites for the Direct Methane to Methanol Conversion. *Phys. Chem. Chem. Phys.* 2020, 22, 18950–18963. DOI: 10.1039/D0CP01257B.
- (26) Chevrier, D. M.; Chatt, A.; Zhang, P.; Zeng, C.; Jin, R. Unique Bonding Properties of the Au<sub>36</sub>(SR)<sub>24</sub> Nanocluster with FCC-Like Core. *J. Phys. Chem. Lett.* **2013**, *4*, 3186–3191. DOI: 10.1021/jz401818c.
- (27) Yang, R.; Morris, D. J.; Higaki, T.; Ward, M. J.; Jin, R.; Zhang, P. New Insights on the Bonding Properties of BCC-like Au<sub>38</sub>S<sub>2</sub>(SR)<sub>20</sub> Nanoclusters from X-Ray Absorption Spectroscopy. *J. Phys. Chem. C* **2018**, *122*, 22776–22782. DOI: 10.1021/acs.jpcc.8b07551.
- (28) Ravel, B.; Newville, M. ATHENA, ARTEMIS, HEPHAESTUS: Data Analysis for X-Ray Absorption Spectroscopy Using IFEFFIT. *J. Synchrotron Radiat.* **2005**, *12*, 537–541. DOI: 10.1107/S0909049505012719.
- (29) Ankudinov, A. L.; Ravel, B.; Rehr, J. J.; Conradson, S. D. Real-Space Multiple-Scattering Calculation and Interpretation of X-Ray Absorption near-Edge Structure. *Phys. Rev. B* **1998**, *58*, 7565–7576. DOI: 10.1103/PhysRevB.58.7565.

- (30) Funke, H.; Scheinost, A. C.; Chukalina, M. Wavelet Analysis of Extended X-Ray Absorption Fine Structure Data. *Phys. Rev. B* **2005**, *71*, 094110. DOI: 10.1103/PhysRevB.71.094110.
- (31) Guliamov, O.; Frenkel, A. I.; Menard, L. D.; Nuzzo, R. G.; Kronik, L. Tangential Ligand-Induced Strain in Icosahedral Au<sub>13</sub>. *J. Am. Chem. Soc.* **2007**, *129*, 10978–10979. DOI: 10.1021/ja0725706.
- (32) Han, W.; Liu, P.; Zheng, M.; Zeng, X. C.; Xu, W. W. Ring Model for Understanding How Interfacial Interaction Dictates the Structures of Protection Motifs and Gold Cores in Thiolate-Protected Gold Nanoclusters. *J. Phys. Chem. Lett.* **2021**, *12*, 3006–3013. DOI: 10.1021/acs.jpclett.1c00544.
- (33) Natarajan, G.; Mathew, A.; Negishi, Y.; Whetten, R. L.; Pradeep, T. A Unified Framework for Understanding the Structure and Modifications of Atomically Precise Monolayer Protected Gold Clusters. *J. Phys. Chem. C* **2015**, *119*, 27768–27785. DOI: 10.1021/acs.jpcc.5b08193.
- (34) Yamazoe, S.; Takano, S.; Kurashige, W.; Yokoyama, T.; Nitta, K.; Negishi, Y.; Tsukuda, T. Hierarchy of Bond Stiffnesses within Icosahedral-Based Gold Clusters Protected by Thiolates. *Nat. Commun.* **2016**, *7*, 10414. DOI: 10.1038/ncomms10414.

# TOC GRAPHICS

